A New Approach to Mineralization of Biocompatible Hydrogel Scaffolds: An Efficient Process toward 3-Dimensional Bonelike Composites

Jie Song,[†,‡] Eduardo Saiz,[†] and Carolyn R. Bertozzi*,[†,‡,§,||]

Contribution from the Materials Sciences Division, Lawrence Berkeley National Laboratory, Departments of Chemistry and Molecular and Cell Biology, and Howard Hughes Medical Institute, University of California, Berkeley, California 94720

Received September 16, 2002 ; E-mail: bertozzi@cchem.berkeley.edu

Abstract: As a first step toward the design and fabrication of biomimetic bonelike composite materials, we have developed a template-driven nucleation and mineral growth process for the high-affinity integration of hydroxyapatite with a poly(2-hydroxyethyl methacrylate) (pHEMA) hydrogel scaffold. A mineralization technique was developed that exposes carboxylate groups on the surface of cross-linked pHEMA, promoting high-affinity nucleation and growth of calcium phosphate on the surface, along with extensive calcification of the hydrogel interior. Robust surface mineral layers a few microns thick were obtained. The same mineralization technique, when applied to a hydrogel that is less prone to surface hydrolysis, led to distinctly different mineralization patterns, in terms of both the extent of mineralization and the crystallinity of the apatite grown on the hydrogel surface. This template-driven mineralization technique provides an efficient approach toward bonelike composites with high mineral-hydrogel interfacial adhesion strength.

Introduction

Bone is a complex tissue that serves many essential functions in the body. It protects organs, provides support and site-of-muscle attachment, generates blood cells, and helps maintain essential ion levels. Structurally, natural bone is a composite of collagen, a protein-based hydrogel template, and inorganic dahilite (carbonated apatite) crystals. The unusual combination of a hard inorganic material and an underlying elastic hydrogel network endows native bone with unique mechanical properties, such as low stiffness, resistance to tensile and compressive forces, and high fracture toughness.[1] Throughout the cavities of bone, there are bone cells and a myriad of soluble factors and extracellular matrix components that are constantly involved with the bone formation and remodeling process.[2] The unique biological functions and mechanical properties of bone are appealing to materials scientists, engineers, and clinicians for a variety of applications, yet the complex nature of bone's structure has hindered real biomimetic design of artificial bonelike materials for a broad range of applications including the treatment of bone defects.

Current artificial materials used in the fabrication of orthopedic implants, metals, ceramics, or polymers, were originally developed for nonbiological applications. Although they could provide an immediate solution for many patients, the long-term outcomes of these implants are not satisfactory. First, these materials exhibit serious mechanical property mismatches with natural bone tissues, which can cause stress shielding and lead to bone resorption when the material has a higher Young's modulus than bone.[3] Very often, revision surgery will be required to follow up the initial implantation.[4] A second major limitation of traditional bone implants is the lack of interaction between these implants and their tissue environment. These materials typically do not bear any functionalities that encourage communication with their cellular environment and, therefore, can only be categorized as bio-inert, far from being bioactive.[5] These "static" implants are not capable of effectively triggering the healing cascade upon surgical implantation, therefore limiting the potential for tissue attachment and in-growth.

The development of a new generation of bonelike composite materials with improved mechanical properties and enhanced biocompatibility calls for a biomimetic synthetic approach using natural bone as a guide. It is suggested that in natural bone synthesis, the biomineralization process starts with the formation of poorly crystalline calcium apatites[6] (preceded by possible transient amorphous calcium phosphates), which are then modified through crystalline phase transitions to form the more stable mature bone apatites with increased crystallinity.[7] During these crystalline phase transitions, acidic extracellular matrix proteins that are attached to the collagen scaffold play important

† Materials Sciences Division, Lawrence Berkeley National Laboratory.
‡ Department of Chemistry, University of California, Berkeley.
§ Department of Molecular and Cell Biology, University of California, Berkeley.
|| Howard Hughes Medical Institute, University of California, Berkeley.
(1) Weiner, S.; Wagner, H. D. *Annu. Rev. Mater. Sci.* **1998**, *28*, 271−298.
(2) Sikavitsas, V. I.; Temenoff, J. S.; Mikos, A. G. *Biomaterials* **2001**, *22*, 2581−2593.

(3) Black, J. *Biological Performance of Materials: Fundamentals of Biocompatibility*, 3rd, rev. and expanded ed.; Marcel Dekker: New York, 1999.
(4) *National Materials Advisory Board Newsletter*, 1997.
(5) Willmann, G. *Adv. Eng. Mater.* **1999**, *1*, 95−105.
(6) Buckwalter, J. A.; Glimcher, M. J.; Cooper, R. R.; Recker, R. *J. Bone Joint Surg.-Am. vol.* **1995**, *77A*, 1256−1275.
(7) Mann, S. *Biomineralization: Principles and Concepts in Bioinorganic Materials Chemistry*; Oxford University Press: New York, 2001.

templating and inhibitory roles.[8,9] Presumably, the acidic groups serve as binding sites for calcium ions and align them in an orientation that matches the apatite crystal lattice.[10,11] The detailed mechanism of the formation and remodeling of natural bone has long been a debate and is still subject to intensive investigations. However, it is clear that template-driven biomineralization, regulated by a number of extracellular matrix components and the participation of bone cells, plays an important role in formation of the highly integrated composite structure of bone. This is the critical feature that the biomimetic synthesis of artificial bone should emulate. We hypothesize that this can be realized by the generation of functional polymer scaffolds displaying surface ligands that mimic critical extracellular matrix components known to direct template-driven biomineralization, or to stimulate or assist cell adhesion, proliferation, migration, and differentiation.[12–15] Ideally, such 3-dimensional scaffolds should also possess proper physical properties, such as desired porosity and water retention ability, to allow both pre-implantation cell seeding and post-implantation tissue ingrowth.

There has been considerable effort to mimic bone by the mineralization of polymer films with hydroxyapatite (HA) (Ca_{10}-$(PO_4)_6(OH)_2$), the major inorganic component of natural bone. This is usually attempted through the time-consuming incubation of substrates with simulated body fluid (SBF).[16] This leads to slow growth of crystalline or amorphous biominerals that exhibit poor adhesion and lack a structural relationship with the substrate.[16–18] Efforts aimed at improving the interface of HA with polymers include the use of silane coupling agents,[19,20] zirconyl salts,[21] polyacids,[22,23] and isocyanates.[24,25] Recently, chemical treatment of biodegradable poly(lactide-*co*-glycolide) films with aqueous base has been shown to facilitate the growth of crystalline carbonate apatite on the surface.[26] Both the morphology and the thickness of the resulting crystalline apatite layer, however, suggest that it will suffer from inadequate interfacial adhesion (between the mineral and the polymer substrate) and poor mechanical properties. Overall, composite materials that integrate organic scaffolds and HA, and demonstrate the level of integration of natural bone, have not yet been achieved.

Hydrogel polymers are particularly appealing candidates for the design of highly functional tissue engineering scaffolds.[27,28] The intrinsic elasticity and water retention ability of synthetic hydrogels resemble those of natural hydrogels, such as collagen matrices that are prevalent as structural scaffolds in various connective tissues including bone.[27] The porosity of synthetic hydrogels may be controlled by various techniques including solvent casting/particulate leaching,[29,30] phase separation,[31] gas foaming,[32] solvent evaporation,[33] freeze-drying,[34] and blending with non-crosslinkable linear polymers[35] to afford a range of mechanical properties. Another important feature of hydrogels is that they can be assembled in 3-dimensional form displaying multiple functional domains through copolymerization of different monomers. The polymerization chemistry is water compatible, allowing incorporation of polar ligands such as anionic peptides that mimic the acidic matrix proteins regulating mineral growth, and biological epitopes such as the tripeptide RGD[36–38] that promote cellular adhesion.

Poly(2-hydroxyethyl methacrylate), or pHEMA, is one of the most well-studied synthetic hydrogel polymers.[39] With its high biocompatibility, pHEMA and its functionalized copolymers have become some of the most widely used synthetic hydrogels in tissue engineering. Applications include ophthalmic devices (e.g., contact lens),[40,41] cartilage replacements,[42] bonding agents in dental resins and bone cements,[43–45] and various drug delivery vehicles.[46,47] One of the major challenges for its application as a 3-dimensional scaffold of artificial bonelike materials, however, is to realize a high-affinity integration of inorganic minerals with the organic pHEMA-based scaffold. This will be required to achieve a composite material with unique mechanical

(8) Raj, P. A.; Johnson, M.; Levine, J. M.; Nancollas, H. G. *J. Biol. Chem.* **1992**, *267*, 5968–5976.

(9) Clark, R. H.; Campbell, A. A.; Klumb, L. A.; Long, C. J.; Stayton, P. S. *Calcif. Tissue Int.* **1999**, *64*, 516–521.

(10) Addadi, L.; Weiner, S. *Proc. Natl. Acad. Sci. U.S.A.* **1985**, *82*, 4110–4114.

(11) George, A.; Bannon, L.; Sabsay, B.; Dillon, J. W.; Malone, J.; Veis, A.; Jenkins, N. A.; Gillbert, D. J.; Copeland, N. G. *J. Biol. Chem.* **1996**, *271*, 32 869–32 873.

(12) Shea, L. D.; Smiley, E.; Bonadio, J.; Mooney, D. J. *Nat. Biotechnol.* **1999**, *17*, 551–554.

(13) Lee, K. Y.; Peters, M. C.; Anderson, K. W.; Mooney, D. J. *Nature* **2000**, *408*, 998–1000.

(14) Mann, B. K.; Schmedlen, R. H.; West, J. L. *Biomaterials* **2001**, *22*, 439–444.

(15) Luo, Y.; Dalton, P. D.; Shoichet, M. S. *Chem. Mater.* **2001**, *13*, 4087–4093.

(16) Kokubo, T. *Acta Mater.* **1998**, *46*, 2519–2527.

(17) Rhee, S.-H.; Tanaka, J. *Biomaterials* **1999**, *20*, 2155–2160.

(18) Saiz, E.; Goldman, M.; Gomez-Vega, J. M.; Tomsia, A. P.; Marshall, G. W.; Marshall, S. J. *Biomaterials* **2002**, *23*, 3749–3756.

(19) Labella, R.; Braden, M.; Deb, S. *Biomaterials* **1994**, *15*, 1197–1200.

(20) Dupraz, A. M. P.; de Wijn, J. R.; vander Meer, S. A. T.; de Groot, K. *J. Biomed. Mater. Res.* **1996**, *30*, 231–238.

(21) Misra, D. N. *J. Dent. Res.* **1985**, *12*, 1405–1408.

(22) Bradt, J.-H.; Mertig, M.; Teresiak, A.; Pompe, W. *Chem. Mater.* **1999**, *11*, 2694–2701.

(23) Liu, Q.; de Wijn, J. R.; Bakker, D.; van Toledo, M.; van Blitterswijk, C. A. *J. Mater. Sci.-Mater. Med.* **1998**, *9*, 23–30.

(24) Liu, Q.; de Wijn, J. R.; van Blitterswijk, C. A. *J. Biomed. Mater. Res.* **1998**, *40*, 257–263.

(25) Liu, Q.; de Wijn, J. R.; van Blitterswijk, C. A. *J. Biomed. Mater. Res.* **1998**, *40*, 358–364.

(26) Murphy, W. L.; Mooney, D. J. *J. Am. Chem. Soc.* **2002**, *124*, 1910–1917.

(27) Peppas, N. A. *Hydrogels in Medicine and Pharmacy*; CRC Press: Boca Raton, 1986.

(28) Lee, K. Y.; Mooney, D. J. *Chem. Rev.* **2001**, *101*, 1869–1879.

(29) Holy, C. E.; Shoichet, M. S.; Davies, J. E. *J. Biomed. Mater. Res.* **2000**, *51*, 376–382.

(30) Mooney, D. J.; Cima, L.; Langer, R.; Johnson, L.; Hansen, L. K.; Ingber, D. E.; Vacanti, J. P. *Mater. Res. Soc. Symp. Proc.* **1992**, *252*, 345–352.

(31) Klawitter, J. J.; Hulbert, S. F. *J. Biomed. Mater. Res. Symp.* **1971**, *2*, 161–229.

(32) Harris, L. D.; Kim, B.-S.; Mooney, D. J. *J. Biomed. Mater. Res.* **1998**, *42*, 396–402.

(33) Mikos, A. G.; Sarakinos, G.; Leite, S. M.; Vacanti, J. P.; Langer, R. *Biomaterials* **1993**, *14*, 323–330.

(34) Whang, K.; Healy, K. E. In *Methods of Tissue Engineering*; Atala, A., Lanza, R. P., Eds.; Academic Press: San Diego, San Francisco, New York, Boston, London, Sydney, Tokyo, 2002; pp 697–704.

(35) Brauker, J. H.; Carr-Brendel, V. E.; Martinson, L. A.; Crudele, J.; Johnston, W. D.; Johnson, R. C. *J. Biomed. Mater. Res.* **1995**, *29*, 1517–1524.

(36) Massia, S. P.; Hubbell, J. A. *Ann. N. Y. Acad. Sci.* **1990**, *589*, 261–270.

(37) Barrera, D. A.; Zylstra, E.; Lansbury, P. T.; Langer, R. *J. Am. Chem. Soc.* **1993**, *115*, 11 010–11 011.

(38) Ratner, B. D. *J. Mol. Recognit.* **1996**, *9*, 617–625.

(39) Kost, J.; Langer, R. In *Hydrogels in Medicine and Pharmacy*; Peppas, N., Ed.; CRC Press: Boca Raton, 1987; Vol. III, p 95.

(40) Phillips, A. J.; Stone, J. *Contact Lenses*; Butterworth & Co.: London, Boston, 1989.

(41) Kidane, A.; Sxabocsik, J. M.; Park, K. *Biomaterials* **1998**, *19*, 2051–2055.

(42) Oxley, H. R.; Corkhill, P. H.; Fitton, J. H.; Tighe, B. J. *Biomaterials* **1993**, *14*, 1064–1072.

(43) Vermeiden, J. P. W.; Rejda, B. B.; Peelen, J. G. J.; de Groot, K. In *Evaluation of Biomaterials*; Winter, G. D., Leray, J. L., de Groot, K., Eds.; Wiley: New York, 1980; pp 405–411.

(44) Yang, J. M.; You, J. W.; Chen, H. L.; Shih, C. H. *J. Biomed. Mater. Res.* **1996**, *33*, 83–88.

(45) Prati, C.; Mongiorgi, R.; Valdre, G.; Montanary, G. *Clin. Mater.* **1991**, *8*, 137–143.

(46) Lu, S.; Anseth, K. S. *J. Controlled Release* **1999**, *57*, 291–300.

(47) Sefton, M. V.; May, M. H.; Lahooti, S.; Babensee, J. E. *J. Controlled Release* **2000**, *65*, 173–186.

Scheme 1. Urea-Mediated Solution Mineralization of Hydroxyapatite (HA) onto pHEMA Hydrogel Scaffolds[a]
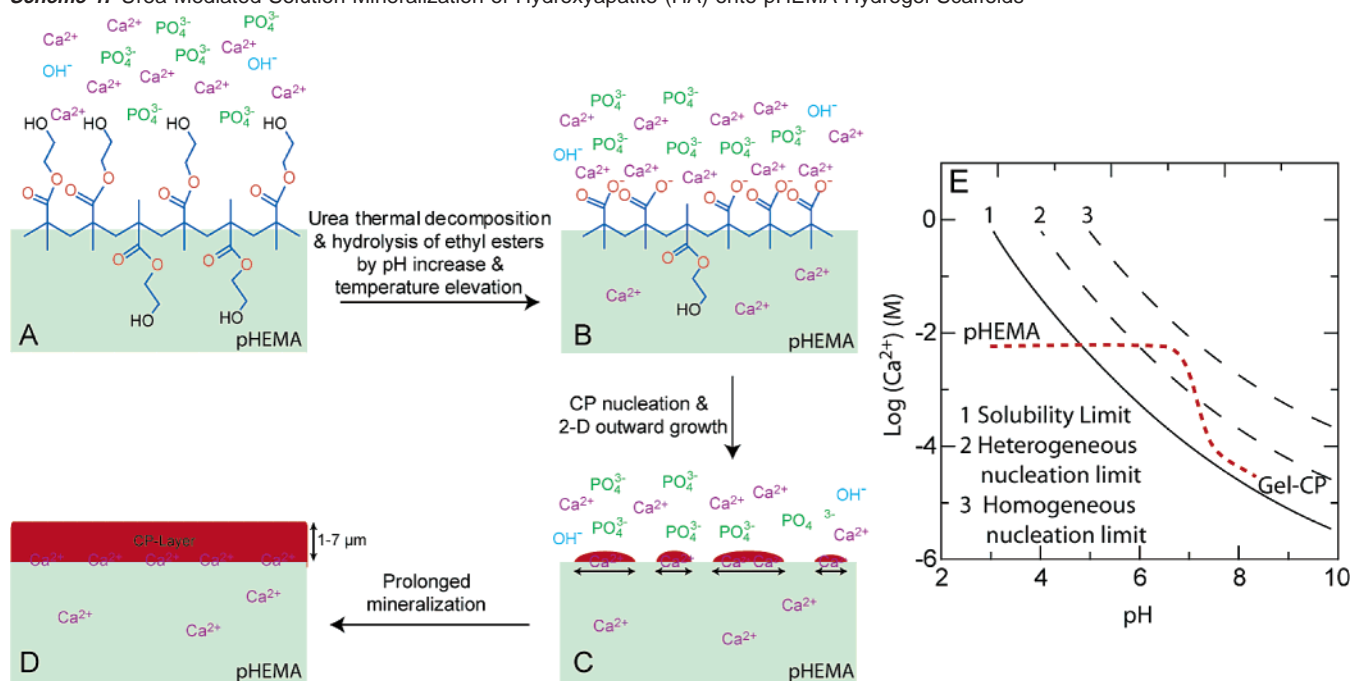
[a] Thermo-decomposition of urea produces a gradual increase in pH, resulting in the hydrolysis of surface 2-hydroxyethyl esters (A) and the precipitation of HA from the aqueous solution. The in situ generated surface carboxylates strongly interact with calcium ions (B) and facilitate the heterogeneous nucleation and 2-dimensional growth of a high-affinity calcium-phosphate (CP) layer on the pHEMA surface (C). Prolonged mineralization allows for the growth of a thicker CP layer that covers the entire hydrogel surface as shown in D. A proposed urea-mediated, pH-dependent HA nucleation and growth behavior from the solution in qualitatively depicted by the red dotted curve shown in E (curve 1, the solubility of HA, was taken from reference 50), guiding the chemical and physical transformation of the pHEMA hydrogel to a highly integrated Gel−CP composite.

properties, biocompatibility and osteophilic interaction with its natural bone environment.

Here, we report the development of a rapid and effective mineralization method that leads to high affinity integration of HA with a pHEMA hydrogel scaffold. This work serves as an important first step toward the development of hydrogel-based biomimetic composite materials. The correlation between the surface properties of hydrogel substrates, the extent of mineralization, the strength of mineral adhesion (at the gel-mineral interface), and the mineral crystallinity was also investigated. This robust mineralization technique, when combined with further incorporation of functional domains of increasing molecular complexity through copolymerization with HEMA, could lead to new generations of composite materials with enhanced tissue-implant interactions. Such a "bottom-up" approach will facilitate our understanding of structure−function relationships in template-driven biomineralization, and help us derive a set of rules to guide future rational design of composite materials.

Results

2-Hydroxyethyl methacrylamide (HEMAm) was synthesized through direct coupling of ethanolamine with methacryloyl chloride under slightly basic (pH 8) conditions. A standard radical polymerization protocol was used for the preparation of pHEMA and pHEMAm.[48] The cross-linker ethylene glycol dimethacrylate (EGDMA) was used at 2%, 5%, and 10% (by weight) to afford pHEMA gels with varied degrees of cross-linking. These gels were found to have same (40%) equilibrium

water content (EWC). All subsequent experiments were carried out with gels cross-linked by 2% EGDMA.

Calcium apatites are known to promote bone apposition and differentiation of mesenchymal cells to osteoblasts.[49] In this work, we chose to use synthetic HA in the fabrication of hydrogel-based bonelike composite materials. HA has limited solubility in water at neutral and basic pH but is highly soluble at acidic pH.[50] On the basis of this property, we employed a urea-mediated solution precipitation technique that has been previously used in the preparation of composite ceramic powders.[51,52] In an adapted protocol, a segment of pHEMA hydrogel was soaked in an acidic solution (pH 2.5−3) of HA containing a high concentration of urea (2 M). As depicted in Scheme 1, upon gradual heating (without stirring) from room temperature to 90−95 °C (within 2 h), urea started to decompose and the pH slowly increased (around pH 8). Under these conditions, some hydrolysis of the 2-hydroxyethyl esters occurred at the hydrogel surface, promoting heterogeneous nucleation and 2-dimensional growth of calcium phosphate (CP) (Scheme 1, A−C). By allowing mineralization to proceed for a longer time after reaching 95 °C (12 h total), a CP layer several microns thick formed over the entire hydrogel surface (Scheme 1D).

There are several notable features of this procedure. First, increasing pH and temperature during the process promotes the

(48) Chilkoti, A.; Lopez, G. P.; Ratner, B. D. *Macromolecules* **1993**, *26*, 4825−4832.

(49) Darimont, G. L.; Cloots, R.; Heinen, E.; Seidel, L.; Legrand, R. *Biomaterials* **2002**, *23*, 2569−2575.
(50) Nancollas, G. H.; Zhang, J. In *Hydroxyapatite and Related Materials*; Brown, P. W., Constantnz, B., Eds.; CRC: Boca Raton, 1994; p pp73.
(51) Blendell, J. E.; Bowen, H. K.; Coble, R. L. *Am. Ceram. Soc. Bull.* **1984**, *63*, 797−801.
(52) De Jonghe, L. C.; He, Y. In *Ceramic Microstructures: Control at the Atomic Level*; Tomsia, A. P., Glaeser, A., Eds.; Plenum Press: New York, 1998; pp 559−565.

hydrolysis of the ethyl ester side chains of pHEMA and leads to the in-situ generation of an acidic surface and a partially acidic interior that has high affinity for calcium ions. Simultaneously, the mineral concentration in the solution undergoes a dramatic change (as the pH rose from 3 to 8) as depicted by the red dotted curve shown in Scheme 1E. Curve 1, adapted from the work of Nancollas et al., depicts the general solubility of hydroxyapatite.[50] Curves 2 and 3 represent qualitative depictions of typical nucleation behavior of calcium phosphates derived from basic nucleation theory reported in the literature.[51,52] The subtle differences in solubility and precipitation behavior of various calcium phosphates are not reflected in this scheme. The high affinity between the calcium ions and the exposed carboxylate groups at the gel surface translates into a low interfacial energy between the hydrogel and calcium phosphate, and consequently, a low energy barrier for the heterogeneous nucleation of mineral on the hydrogel surface (as shown by curve 2 in Scheme 1E). Second, the thermo-decomposition of urea allows a homogeneous variation of pH across the solution, avoiding a sudden local pH change that is commonly observed with strong base-induced precipitation.[52] Third, any homogeneous precipitates that fall on the hydrogel and remain loosely attached to the composite surface can be easily washed away during the workup rinsing. Reproducible urea-mediated mineralization can be achieved by closely monitoring the amount of urea used (affecting the final pH), the heating rate (affecting mineral nucleation and growth rate) and the duration of the process (affecting the extent of mineral coverage on the hydrogel surface). We have shown that heating rates between 0.2 °C/min and 0.5 °C/min will promote the formation of a CP layer that uniformly covers the gel surface.

The hydrolysis of 2-hydroxyethyl esters during the thermo-decomposition of urea was expected to lead to an increase of surface hydrophilicity, which was confirmed by contact angle and EWC measurements. In a mock experiment, a segment of pHEMA gel was thermally treated as described above in a solution containing the same concentration of urea, without the presence of HA. Diiodomethane, a hydrophobic solvent that is known to from stable droplets on hydrophilic materials without noticeable penetration and contact angle hysteresis,[53] was used for measuring contact angles against water on both the treated and untreated pHEMA gels. The contact angle of a diiodomethane droplet on the gel surface was found to increase from 129° to 142° upon the urea-mediated thermal treatment for 2 h. The observed decrease in surface wettability by a hydrophobic solvent is consistent with the postulated in-situ generation of polar surface carboxylates during the urea-mediated mineralization. The hydrolysis also led to a slight increase (2−3%) in the EWC of the gel.

The strong affinity between calcium and the in situ generated acidic surface of pHEMA led to the 2-dimensional outward growth of calcium phosphate from individual nucleation sites (Figure 1A). After 2 h, the circular mineral layers merged and covered the entire surface (Figure 1B). The adhesion strength of the apatite layer to the gel surface was studied by microindentation analysis[54] performed on the surface of the mineral-
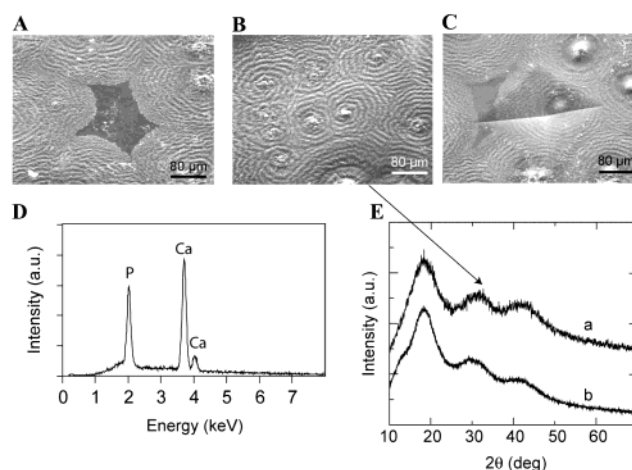

Figure 1. Morphology, crystallinity, and mineral-gel interfacial affinity of calcium phosphate apatite layer grown on the surface of pHEMA after 2 h. (A) SEM showing 2-dimensional circular outward growth of calcium apatite from multiple nucleation sites on the acidic surface of pHEMA. (B) SEM showing the merge of circular mineral layers and the full coverage of the hydrogel surface with calcium apatite. (C) SEM showing an indent formed on the surface of mineralized pHEMA using a Vickers microindenter with a load of 5 N. The calcium phosphate layer did not delaminate. (D) SEM-associated EDS area analysis of the mineral layer shown in micrograph B, confirming the chemical composition and Ca/P ratio (1.6 ± 0.1) that is typical for HA. Synthetic HA was used to calibrate the determination of the Ca/P ratio. (E) X-ray diffraction patterns of the pHEMA composite (a) and unmineralized pHEMA gel (b). The lack of diffraction peaks corresponding to crystalline HA suggests that an amorphous or nanocrystalline layer was formed on the pHEMA surface.

hydrogel composite. No delamination of the mineral layer was observed by SEM even after Vickers indentations with loads of 5−15 N (Figure 1C) which is an indication of good adhesion. The calibrated energy dispersive spectroscopy (EDS) area analysis performed on the mineral surface of the composite revealed a Ca/P ratio (1.6±0.1) similar to that of synthetic HA (Figure 1D).

Most of the flakelike crystal apatite coatings obtained by mineralization in SBF on bioactive glasses, polymer scaffolds or collagen films are not robust and tend to delaminate easily upon drying.[16−18,55] We attempted microindentation analysis with the apatite layers formed on bioglass using SBF mineralization.[18] The minerals crumbled with even very low loadings and are therefore considered not amendable for such analysis. Recently, a modified mineralization approach, involving the use of very high concentrations of SBF and careful control of HCO_3^- concentrations, was used to bind nanosized apatite crystals to commercial metal implants with improved strength.[56,57] However, no mechanical tests that could characterize the interfacial adhesion between these apatites and the metal substrates were reported.

X-ray diffraction (XRD) analysis performed on the mineralized pHEMA composite indicated that the calcium phosphate layer was either nanocrystalline or amorphous. No typical reflections for crystalline HA were observed, with only a few broad reflections (Figure 1E, a) similar to those observed in the hydrogel prior to mineralization (Figure 1E, b). This suggests

(53) Timmons, C. O.; Zisman, W. A. *J. Colloid Interface Sci.* **1966**, *22*, 165−171.
(54) Gomez-Vega, J. M.; Saiz, E.; Tomsia, A. P. *J. Biomed. Mater. Res.* **1999**, *46*, 549−559.

(55) Du, C.; Cui, F. Z.; Zhang, W.; Feng, Q. L.; Zhu, X. D.; de Groot, K. *J. Biomed. Mater. Res.* **2000**, *50*, 518−527.
(56) Barrere, F.; van Blitterswijk, C. A.; de Groot, K.; Layrolle, P. *Biomaterials* **2002**, *23*, 1921−1930.
(57) Barrere, F.; van Blitterswijk, C. A.; de Groot, K.; Layrolle, P. *Biomaterials* **2002**, *23*, 2211−2220.
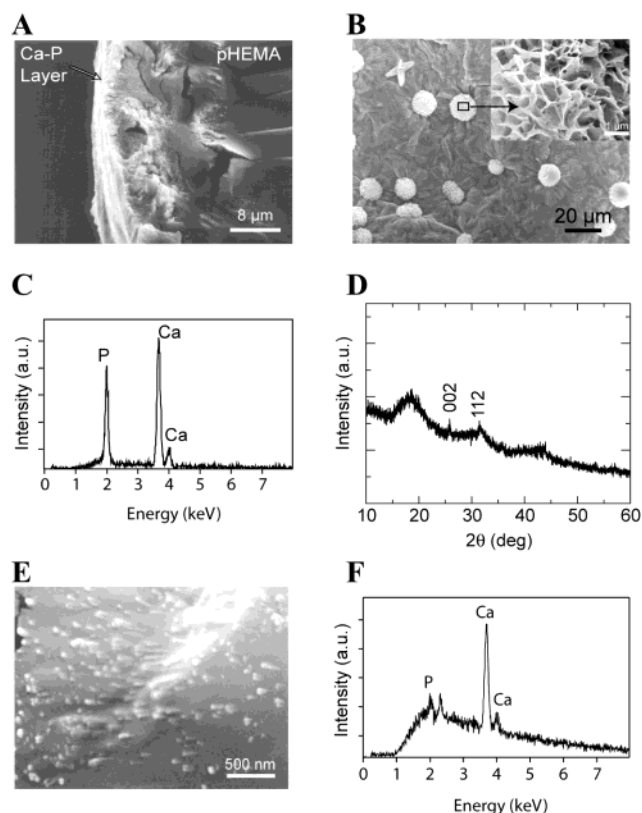
Figure 2. Extended mineralization of pHEMA via a urea-mediated process (12 h): morphology, crystallinity and thickness of calcium apatite layer grown on the hydrogel surface and the calcification of the hydrogel interior. (A) SEM showing the side view of a cross-section of the pHEMA-apatite composite after extended mineralization. The sample stage was tilted 45°. Note the micron scale thickness of the mineral layer and the fine integration at the mineral-gel interface. (B) SEM showing fully mineralized surface of pHEMA after extended mineralization, along with the growth of spherical clusters of crystalline HA from nucleation sites located at the center of circular mineral layers. The inset shows an expanded view of one spherical cluster of HA crystallites. Note the platelike morphology of the calcium apatite crystallites that is commonly observed with crystalline apatites grown on various substrates during SBF mineralization. (C) Calibrated EDS area analysis of the surface mineral layer shown in micrograph B, confirming the chemical composition and Ca/P ratio (1.6 ± 0.1) that is typical of HA. Synthetic HA was used to calibrate the quantification of Ca/P ratio. Same result was obtained on the selected area analysis performed on plate-like HA shown in the inset of micrograph B. (D) X-ray diffraction pattern of pHEMA-HA composite obtained by the urea-mediated mineralization process after 12 hours (the composite shown in Fig. 2B). Peaks corresponding to crystalline HA were detected, suggesting the crystalline nature of the spherical HA grown on top of the calcium apatite coating. Note the preferential alignment along the c-axis. (E) SEM showing the hydrogel interior of the pHEMA-apatite composite. (F) SEM-associated EDS area analysis of the cross-section of pHEMA-apatite composite shown in micrograph E, suggesting significant calcification throughout the hydrogel interior.

that although there is high affinity binding between calcium ions and the in-situ generated surface carboxylates, the spacing, order and/or alignment of these surface anionic ligands do not promote the epitaxial growth of large calcium apatite crystallites along any particular orientation.

By extending mineralization time to 12 h, mineral coatings with thicknesses up to several microns were obtained, with good integration at the mineral-gel interface as shown in a side view image of the composite (Figure 2A). Once the surface was fully covered with the amorphous apatite layer, the growth of HA crystals forming spherical aggregates on top of initial nucleation sites (centers of circular apatite rings) was observed (Figure 2B).

These mineral spheres are composed of platelike crystallites (insert of Figure 2B), a typical morphology observed with the crystalline apatite grown on bioactive glasses polymer substrates or collagen films using SBF mineralization.[16−18,26] EDS analysis performed on the spherical apatite aggregates and XRD performed on the composite material confirmed the expected Ca/P ratio (1.6±0.1) and typical reflections, (002) and (112), for crystalline HA (Figure 2C & 2D).[18] It is worth noting, however, that HA crystals formed by adventitious precipitation often adopt a similar preferential orientation. This suggests that the observation of a preferential alignment of the apatitic crystal lattice in a composite material does not necessarily reflect a specific interaction with the underlying substrate. The cross-section examination of the composite material revealed that there were significant degrees of calcification inside the hydrogel as well, although the degree of phosphate incorporation was limited (Figure 2E & 2F). The extensive calcification of the hydrogel interior may be promoted by the partial hydrolysis of the 2-hydroxyethyl ester side chains inside the pHEMA gel. The growth of calcium apatites inside the pHEMA scaffold is limited by both the space (note that no special technique was applied to promote the formation of a porous hydrogel scaffold in the current study) and the concentration of free anions achieved inside the already partially anionic hydrogel.

To better understand the relationship between surface chemistry of the substrate and the mineralization pattern of the composite material, we applied the same mineralization technique to poly(2-hydroxyethyl methacrylamide) (pHEMAm), a hydrogel that is not prone to side chain hydrolysis under the mineralization conditions. Indeed, an entirely different surface mineral pattern was obtained with pHEMAm gels as shown in Figure 3. The hydrogel was patterned with flowerlike minerals, with much less extensive surface coverage even after 12 h of mineralization. The apatite grown on pHEMAm was crystalline as suggested by both dark field optical image (Figure 3A) and XRD of the composite material (Figure 3B), with major reflections matching with those of crystalline HA. The relative intensities of these reflections suggest a preferential alignment along (002), with the *c*-axis perpendicular to the substrate. SEM micrographs revealed further details of the mineral pattern, showing an upward growth of the bundles of whiskers away from the gel surface (Figure 3C & 3D). This, along with the relatively low surface mineral coverage, is consistent with the decreased affinity between calcium apatite and the neutral hydrogel surface of pHEMAm. EDS analysis performed on the mineral bundles again revealed a Ca/P ratio (1.6±0.1) matching HA (insert of Figure 3D). X-ray elemental mapping of Ca and P (Figure 3E & 3F) showed that the mineral patterns were composed of uniform calcium phosphate apatite. There was no calcification or phosphate incorporation detected at the interior, or on the dark hydrogel surface positions devoid of flowerlike mineral patterns, in agreement with the low-calcium binding nature of pHEMAm. Clearly, surface chemistry plays a very important role in determining both the extent and the pattern of the mineralization (2-D vs 3-D mineral growth). Tightly bound HA prefers to spread on the surface, forming a circularly grown mineral layer that eventually covers the entire gel surface. By contrast, more loosely bound HA, as in the case of pHEMAm, can grow more readily in three dimensions.
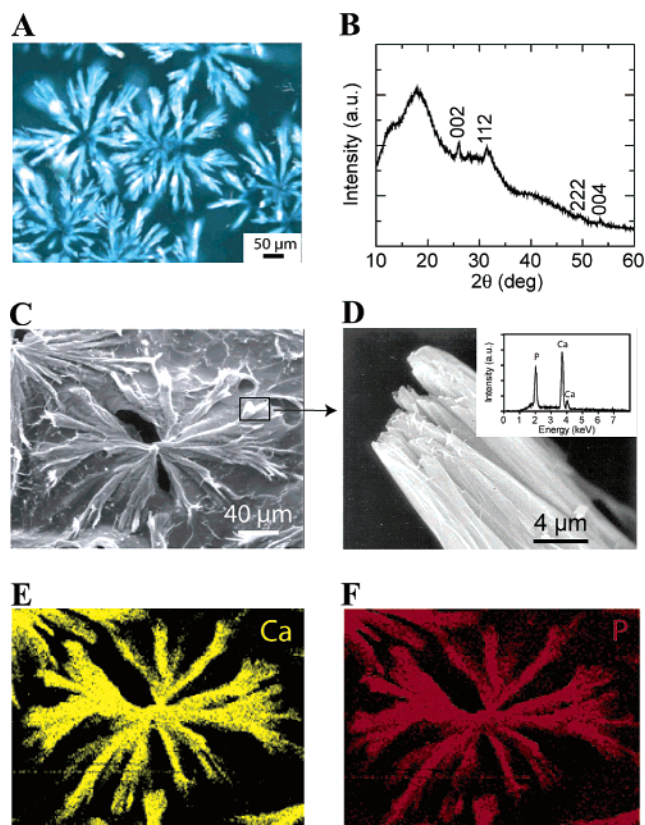
Figure 3. Mineralization of pHEMAm via the urea-mediated process after 2 h: morphology and crystallinity of hydroxyapatite (HA) grown on the hydrogel surface. (A) Dark field optical microscopy image of the mineralized pHEMAm gel. The bright reflection of the flowerlike minerals suggests their crystalline nature. (B) X-ray diffraction pattern of the pHEMAm-mineral composite obtained by the urea mediated mineralization process. Hydroxyapatite peaks can be observed, suggesting the crystalline nature of the minealization. Note the preferential alignment along the c-axis. (C) SEM showing unique surface mineral patterns of pHEMAm-HA composite. (D) SEM showing an expanded view of the tip of one "petal" of the flower-like mineral shown in micrograph C. Note the upward growth of crystal bundles away from the dark hydrogel surface. The inset shows calibrated EDS area analysis of the surface of the composite material, confirming the chemical composition and Ca/P ratio (1.6 ± 0.1) of the surface mineral that is typical of HA. The EDS analysis performed on the un-mineralized hydrogel surface did not detect any Ca or P signal (data not shown). (E) X-ray elemental mapping of Ca with the same sample area shown in micrograph C. Note that there is no calcification of the dark hydrogel background outside of the flowerlike mineral pattern. (F) X-ray elemental mapping of P with the same sample area shown in micrograph C. Note that there is no phosphate incorporation in the dark hydrogel background outside of the flower-like mineral pattern.

Discussion

The mineralization method we describe here takes advantage of the dramatically different solubilities of HA in acidic and basic aqueous media and the chemically labile nature of ester groups of pHEMA in basic media. We employed thermo-decomposition of urea as a facile pH modulator to generate an anionic surface and partially acidic interior of the pHEMA gel. This initiated the heterogeneous nucleation and high-affinity growth of calcium apatite on the gel surface and extensive calcification inside the gel. Overall, this method provides a fast and convenient approach for producing robust pHEMA-calcium apatite composite materials with high quality interfacial integration between the mineral and the polymer substrate. Furthermore, this approach provides a foundation for integrating high-affinity template-driven biomineralization with the versatile

properties of 3-dimensional hydrogel scaffolds, and opens the door for future application of pHEMA in the design of functionalized bone replacements.

As represented in Scheme 1, the formation of the robust CP layer on the hydrolyzed surface of pHEMA gel is driven by the lower interfacial energy between the carboxylate rich gel surface and the mineral. Once the pH and temperature reach an equilibrium and the gel surface is fully covered with an initial nanocrystalline or amorphous CP layer of a critical thickness, the growth of CP composed of large platelet crystallites that are easily detectable by XRD becomes energetically favorable. Maintaining the final pH of the mineralization solution at around 8 prevents competing homogeneous precipitation from the medium.

The distinctly different mineralization patterns observed on pHEMA and pHEMAm gels using the same mineralization procedure indicates that the chemical nature of the hydrogel dictates the affinity and extent of mineralization. Other surfaces, such as bioglass have been shown to mineralize with crystalline CP.[16,18] However, crystalline apatite growth is not necessarily a result of template-driven mineralization. Instead, it could occur even with poor substrate-mineral interaction resulting from a random crystallization process. Existing mineralization techniques applied to a vast range of substrates using SBF often result in the formation of similar crystalline apatite coatings composed of either platelike or flakelike apatite crystals.[16,18,26] The formation of such loosely covered crystalline mineral layers indicates limited substrate-mineral interaction. That is, such mineral nucleation and growth are not highly surface dependent or strictly template driven. The precipitation is instead promoted by the subtle local pH changes and/or local ion saturation induced by the substrate. Similarly, in this study, the growth of crystalline calcium apatite spheres after saturation of the initial mineral coating is surface independent. Our results suggest that a true template driven biomineralization process requires the establishment of direct and extensive mineral-substrate contact, as we observed between pHEMA and HA. High affinity 2-dimensional mineral growth at the substrate-mineral interface reflects such extensive interactions.

In natural bone synthesis, it has been suggested that the biomineralization process starts with the formation of transient amorphous calcium phosphates (although the direct detection of these transient precursors is difficult using static techniques such as XRD and solid-state NMR[58,59]) and poorly crystalline apatites.[59,60] These precursors then undergo several crystalline phase transitions, such as brushite, octacalcium phosphate, and tricalcium phosphate, before the more stable bone apatites with higher crystallinity finally form.[7] This complex process is mediated by the dissolution and saturation of mineral ions at the mineral-substrate interface, as well as bone matrix proteins. Two different paradigms can be envisioned that mimic natural bone synthesis in the fabrication of bone-like composite materials. One could start with a highly ordered molecular template to promote template-driven mineralization of crystalline apatites.[61] Indeed, this approach has been pursued in the context

(58) Roberts, J. E.; Heughebaert, M.; Heughebaert, J. C.; Bonar, L. C.; Glimcher, M. J.; Griffin, R. G. *Calcif. Tissue Int.* **1991**, *49*, 378−382.
(59) Roberts, J. E.; Bonar, L. C.; Griffin, R. G.; Glimcher, M. J. *Calcif. Tissue Int.* **1992**, *50*, 42−48.
(60) Kim, H. M.; Rey, C.; Glimcher, M. J. *Calcif. Tissue Int.* **1996**, *59*, 58−63.
(61) Hartgerink, J. D.; Beniash, E.; Stupp, S. I. *Science* **2001**, *294*, 1684−1688.

of nanotube composites, using supramolecular aggregates of peptide-amphiphiles bearing biomimetically designed mineral nucleating ligands. Alternatively, one could start with composite materials with properly adhered amorphous or nanocrystalline osteophilic mineral compositions and encourage nature's remodeling pathway to eventually take over and engineer the initial mineral phase. It is this latter approach that may be enabled by the method presented herein.

In addition to strong adhesion at the gel−mineral interface, the composites generated here have a HA layer with a structure and thickness that are ideal for bone implant applications. Analysis of calcium phosphate coatings on titanium implants has shown that resorption of the coating occurs mostly in the less organized apatite region and stops where the coating has higher crystallinity.[49] Thus, amorphous or nanocrystalline HA coatings as we have achieved should promote resorption and bone integration. In addition, earlier studies suggest that a thin layer of HA with thickness on the order of 1−7 μm, as we have achieved, provides a sufficient HA resorption time frame to allow a progressive bone contact with the implant substrate and is, therefore, ideal for inducing integration of the material into natural bone.[49] By contrast, classical plasma spray techniques applied to metal implants[62] produce HA coatings over 50 μm thick. The favorable properties of the hydrogel-calcium apatite composite obtained using the approach described here may potentially maximize the chance for initiating in vivo remodeling cascades and subsequent positive tissue-implant integration. More in vitro and in vivo studies will have to be performed before the real value of composites formed using this approach can be estimated. In addition, the porosity of the hydrogel scaffold has not yet been tuned, although many available techniques (e.g., solvent casting/particulate leaching, gas foaming and freeze-drying)[29,30,32,34] can be applied to this effort. Such modifications could further enhance the degree of mineralization at the interior of the composite material and allow deeper tissue ingrowth. These applications and extensions of the method are presently under investigation.

Experimental Protocols

Synthesis. 2-Hydroxyethyl methacrylamide (HEMAm). To 20 mL of ice-cold methanolic solution of ethanolamine (2 mL, 33 mmol) was slowly added 3.26 mL (34 mmol) of methacryloyl chloride (diluted in 20 mL of THF). Potassium hydroxide (1 M, aqueous) was added to maintain the solution pH at 8−9 throughout the reaction. The mixture was warmed to room temperature over 2 h and stirred for another 2 h before it was quenched by the addition of hydrochloric acid to a final pH of 5. The product was concentrated and redissolved in cold ethanol to precipitate the potassium chloride salt. After silica gel flash chromatography purification (chloroform: methanol/9:1), the product (R_f 0.5) was isolated in 95% yield. ^{1}H NMR (500 MHz, CD$_3$OD): δ 7.10 (1H, b), 5.55 (1H, s), 5.16 (1H, s), 3.51 (2H, t, $J = 5.5$ Hz), 3.25 (2H, q, $J = 5.0$ Hz), 1.76 (3H, s); ^{13}C NMR (125 MHz, CD$_3$OD): δ 169.31, 139.06, 119.82, 60.71, 41.96, 18.09; HRMS FAB$^+$ (NBA): C$_6$O$_2$NH$_{12}$ [M+H]$^+$, Calcd, 130.0868. Found 130.0868.

Hydrogel Preparation. 2-Hydroxyethyl methacrylate (HEMA) was purchased from Aldrich and purified via distillation under reduced pressure prior to use. In a typical procedure, 500 mg of hydrogel monomer was combined with 10 μL of ethylene glycol dimethacrylate, 100 μL of Milli-Q water and 150 μL of ethylene glycol. To this mixture was added 50 μL each of an aqueous solution of sodium metabisulfite (150 mg/mL) and ammonium persulfate (400 mg/mL). The well-mixed viscous solution was then poured into a glass chamber made by microscope slides and allowed to stand at room temperature overnight. The gels (5.5 cm × 1.5 cm × 1 mm) were then soaked in Milli-Q water for 2−3 d, with daily exchange of freshwater, to ensure the complete removal of unreacted monomers before they were used for mineralization and further physical characterizations.

Equilibrium Water Content (EWC) Measurements. The EWC at room temperature is defined as the ratio of the weight of water absorbed by a dry hydrogel to the weight of the fully hydrated hydrogel. The amount of water absorbed by the hydrogel is determined from the weight of a freeze-dried gel (W_d) and the weight of the corresponding hydrated gel (W_h) according to the following equation

$$EWC\ (\%) = [(W_h - W_d)/W_h] \times 100$$

Contact Angle Measurements. The contact angles of diiodomethane droplets against water on hydrogels were measured using the sessile drop method. A 3−5 μL droplet of diiodomethane was placed on the surface of a segment of hydrogel submerged in water. The static contact angles were measured with a Goiniometer from both sides of the droplet within 10 s after depositing the drop, and the values were averaged. The contact angle was found to be 129° and 142° for the prehydrolyzed pHEMA and posthydrolyzed pHEMA, respectively.

Mineralization of Hydrogels with the Urea-Mediated Process. HA (2.95 g) was suspended into 200 mL of Milli-Q water with stirring, and 2 M HCl was added sequentially until all the HA suspension was dissolved at a final pH of 2.5−3. Urea (24 g) was then dissolved into the solution to reach a concentration of 2 M. Each hydrogel strip was then immersed into 50 mL of the acidic stock HA solution containing urea. The solution was slowly heated without stirring to 90−95 °C (within 2 h) and maintained at that temperature overnight when necessary. The final pH was around 8.

Structural Characterizations. Mineralized hydrogel strips were repeatedly washed in water to remove loosely attached minerals and soluble ions before they were freeze-dried for further structural analyses and mechanical characterization. The surface microstructures and crystallinity of the materials grown on the surface and inside of the hydrogel were analyzed by scanning electron microscopy (SEM) with associated energy dispersive spectroscopy (EDS) and X-ray powder diffraction (XRD).

SEM-EDS. All SEM micrographs of freeze-dried hydrogels and hydrogel-mineral composites were obtained with a ISI-DS 13OC dual stage SEM with associated EDS. Samples were coated with either Au or Pt on a BAL-TEC, SCD 050 sputter coater to achieve optimal imaging results, or coated with carbon for EDS analysis. The imaging and analysis of composite materials were performed at 15 kV, and those of hydrogels were performed under reduced voltage (8−12 kV). The determination of Ca/P ratios of all composite materials were based on calibration using a standard synthetic HA sample.

(62) de Groot, K.; Geesink, R.; Klein, C. *J. Biomed. Mater. Res.* **1987**, *21*, 1375−1381.

XRD. The presence and overall orientation of crystalline phases in the precipitated mineral layers were evaluated by XRD with a Siemens D500 instrument using Cu Kα radiation.

Evaluation of Mineral-Hydrogel Interfacial Adhesion. To evaluate the adherence of the mineral layers attached to pHEMA hydrogels, the relative crack resistance was qualitatively evaluated by indentation. The indentation test was performed using a Vickers indentor (Micromet, Buehler, Ltd., USA) that has a diamond pyramidal tip with a 136° angle between its faces. Loads from 5 to 15 Newtons were applied for 20 s for each measurement. After indentation, the samples where analyzed by SEM to check for delamination. Lack of delamination is an indication of strong adhesion between the mineral layer and the hydrogel substrate.

JA028559H